Journal of The Electrochemical Society, **155** (3) D244-D250 (2008)
0013-4651/2008/155(3)/D244/7/$23.00 © The Electrochemical Society

Dynamics of Copper Deposition onto Silicon by Galvanic Displacement

Calvin P. daRosa,* Enrique Iglesia,[z] and Roya Maboudian[z]

Department of Chemical Engineering, University of California, Berkeley, Berkeley, California, 94720, USA

Copper was deposited onto silicon rotating-disk electrodes in 3.0 M HF to determine the effects of boundary-layer mass transfer and surface reaction kinetics on Cu deposition rates. For all solution compositions tested ($[CuSO_4] = 0.0010 - 0.020$ M, $[HF] = 3.0$ M), the Cu deposition rate was proportional to the concentration of Cu^{2+} and was under mixed diffusion and surface kinetic control. HF was used to dissolve oxidized Si, and a stoichiometry of one Cu atom deposited for each Si atom that is oxidized and dissolved was deduced from a combination of UV-visible spectroscopy and mass change experiments. These results indicate that Si dissolves as Si^{2+}, not Si^{4+}, as is commonly assumed for galvanic displacement. Mixed-potential theory was used to further analyze the reaction mechanism, and deposition rates and open-circuit potential values predicted from this method agreed well with experimental results during the initial stages of Cu deposition. Deposition rates decreased abruptly when film thicknesses exceeded 150 nm, and optical microscopy revealed buckling in these Cu films. This buckling occurred in response to compressive stresses in the films and decreased deposition rates by partially detaching Cu films from the Si substrate.
 [DOI: 10.1149/1.2829907]

Manuscript submitted September 19, 2007; revised manuscript received November 21, 2007.
Available electronically January 23, 2008.

In galvanic displacement, Cu^{2+} ions are reduced and deposited onto Si substrates with electrons provided by oxidation and dissolution of Si. This method is commonly used to deposit Cu because of its favorable reduction potential [$E^o = 0.34$ V vs a normal hydrogen reference electrode (NHE)][1,2]

$$Cu^{2+} + 2e^- \rightarrow Cu \quad [1]$$

Previous studies of Cu deposition onto Si in stagnant solutions concluded that Cu^{2+} diffusion through the mass-transfer boundary layer limits film growth,[3,4] but this has not been tested under other hydrodynamic conditions. Rotating disk electrodes (RDEs) have been used previously to separate the effects of mass transfer from surface reaction kinetics for galvanic displacement on metals such as Ni and Zn,[5,6] but not for Si substrates. Here, Cu is deposited on Si RDEs to measure the effects of mass transfer and chemical reaction rates on the dynamics of Cu deposition.

Si can dissolve as either Si^{2+} or Si^{4+}, depending on the concentration of fluoride species and on the oxidation rate.[7] Si is first oxidized to Si^{2+}, which remains on the surface and reacts further by one of two parallel pathways. In the first, Si^{2+} is dissolved by fluoride species, followed by further oxidation in solution[8,9]

$$Si^{2+} + 2F^- \rightarrow SiF_2 \quad [2]$$

$$SiF_2 + 4F^- + 2H^+ \rightarrow SiF_6^{2-} + H_2 \quad [3]$$

Alternatively, Si^{2+} surface species can be further oxidized to Si^{4+}, which is then dissolved[8]

$$Si^{2+} \rightarrow Si^{4+} + 2e^- \quad [4]$$

$$Si^{4+} + 6F^- \rightarrow SiF_6^{2-} \quad [5]$$

The valence of the solvated species is thus determined by the relative rates of oxidation and dissolution of surface Si^{2+} species; Si^{2+} dissolution is favored when dissolution (Eq. 2) is more rapid than oxidation (Eq. 4). This occurs in more concentrated HF solutions and when oxidation rates are relatively low.[8] The surface structure of Si is strongly affected by the mode of dissolution. Porous silicon forms during divalent dissolution, while a smooth electropolished surface forms during tetravalent dissolution.[7,8,10] Si^{4+} dissolution has been proposed for galvanic displacement of Cu on Si in previous studies.[11-13] The few quantitative measurements of Si dissolution rates during galvanic displacement, however, suggest that Si^{2+} dissolution is the prevalent Si oxidation pathway.[14,15] Si^{2+} dissolution has been proposed for Ni deposition onto Si, without direct evidence.[16] In this study, UV-visible spectroscopy is used to measure Si dissolution rates during galvanic displacement and identify the dominant Si dissolution pathway.

Open-circuit potential (OCP) measurements can be used to identify rate-limiting elementary processes in each half-reaction during galvanic displacement.[17] At this potential, sometimes denoted as the mixed potential, electrons are consumed in the reduction half-reaction at the same rate as they are formed in the oxidation half-reaction.[18] OCP transients have been measured during galvanic deposition of Cu on rotating Zn and Al disks,[6,19] as well as on Si in stagnant solutions.[20-22] These measurements allowed sensitive detection of changes in reaction conditions, but they were not used to quantitatively assess the deposition mechanism. Here, we use mixed-potential theory to interpret OCP measurements in terms of the proposed deposition mechanism.

Experimental

Single-crystalline p-type Si(100) wafers (resistivity = 10–20 Ω cm; Wafernet, Inc.) were used as substrates for Cu deposition. Wafers were cleaned by sonication (Fisher FS-28, 43 kHz) in acetone (Fisher, 99.5%) for 600 s and then rinsed with deionized water (~18 MΩ cm) and dried in N_2 flow. Residual adsorbed organic impurities were removed by reactions with ozone under ultraviolet irradiation (254 nm, 0.028 W cm^{-2}) for 600 s (UVO cleaner model 42; Jelight Company, Inc.). Oxide films were then dissolved in 6 M HF (EMD Chemicals, 48%) for 120 s. Si wafers were cut into smaller chips, and the back surface of each was scratched with a diamond point and coated with colloidal Ag (60% Ag in 1-methoxy-2-propanol; Ted Pella, Inc.) to ensure electrical contact for OCP measurements. Ag coatings were allowed to stand for at least 0.5 h to dry before deposition experiments.

Si chips were attached to the end of the rotating shaft of an analytical rotator (model A5R2, Pine Instruments) for Cu deposition experiments. Angular velocities were varied between 20 and 250 rad s^{-1} (~200–2500 rpm) and deposition times between 10 and 1800 s. Aqueous HF (3.0 M) and $CuSO_4 \cdot 5H_2O$ (0.0010–0.020 M, Fisher, 99.3%) solutions were used. Solutions were sparged with N_2 (Matheson Tri Gas, 99.999%, 10^2 cm^3 s^{-1}) for 300 s before deposition and kept under a N_2 blanket during deposition. After deposition, the films were rinsed with deionized water for ~60 s and dried in flowing N_2. In contrast with some earlier reports,[21,23,24] deposition rates were not strongly affected by illumination, and all experiments reported below were performed in ambient light and room temperature. OCP values were measured with a high-impedance voltmeter (Keithley 2400 SourceMeter) using Hg/Hg_2SO_4 (REF621,

* Electrochemical Society Student Member.
[z] E-mail: iglesia@berkeley.edu; maboudia@berkeley.edu

Radiometer Analytical) as the reference electrode. Data were recorded using LabTracer 2.0 software at sampling rates of 14 Hz.

Atomic force microscopy (AFM) measurements were performed with a Digital Instruments MultiMode III system using tapping mode. Film thicknesses were measured by scratching Cu films with Teflon tweezers to expose the underlying Si and imaging the resulting step using 25 μm scans. High ratios of solution volume to Si surface area (100 cm^3 solution, 1 cm^2 Si area) were used in these experiments to maintain Cu^{2+} concentrations nearly constant during film growth. Optical microscopy was performed using a Mitutoyo Finescope at 20× magnification, and images were recorded using a charge-coupled device camera (Sony SSC-C370).

In separate experiments, Cu deposition rates were measured from UV-visible spectra (Cary 400 Spectrometer) of the solutions. Low ratios of solution volume to Si surface area (<10 cm^3 solution cm^{-2} Si) were used here to produce detectable changes in Cu^{2+} concentration. Cu was deposited onto rotating Si electrodes, and 1 cm^3 aliquots of solution were removed at regular time intervals. Following deposition, the Cu^{2+} concentration in each aliquot was measured from its absorbance at 800 nm. After Cu^{2+} analysis, the Si^{4+} content in each solution aliquot was measured by forming molybdosilicic acid using the following procedure.[25] First, each aliquot was diluted ninefold with saturated solutions of boric acid (Allied Chemical, 99.8%). Two cm^3 of this solution was added to 1 cm^3 of a solution containing a 2.5:2.5:3 mixture of 1 M H_2SO_4 (EMD, 95%): $(NH_4)_2MoO_7$ (Alfa Aesar, 10% w/v in H_2O):acetone (Fisher, 99.6%). The solutions were then allowed to stand for 0.5 h at ambient conditions, and their Si content was determined from the absorbance at 400 nm. Si concentrations were calibrated by adding known amounts of H_2SiF_6 (Alfa Aesar, 35% w/w aqueous solution) to 3.0 M HF solutions.

The masses of Cu deposited and Si dissolved were also measured directly for the samples used in UV-visible experiments. First, the Si mass was measured (±0.1 mg) using an analytical balance (model A-250, Denver Instrument Company). After deposition, the sample was rinsed, dried, and weighed again. The Cu film was then dissolved in 1 M HNO_3 (Fisher, 69.5%) for 60 s and the Cu-free Si sample was weighed again. The amount of Si dissolved during galvanic displacement equaled the difference between this final mass and the initial mass. The mass of Cu deposited equaled the difference in mass before and after dissolving the Cu film. These results agreed with those determined from UV-visible spectra to within 20%.

Si wafers with silicon carbide (SiC) features were also used to determine the rates of Cu deposition and Si dissolution.[26,27] SiC features (~80 nm above the initial Si surface) serve as reference heights, because no dissolution or deposition occurs on these surfaces. The height differences between Si and SiC were first measured at 10–15 locations on the sample. These measurements were repeated at the same locations following Cu deposition, and again after Cu dissolution in HNO_3, as in the mass measurements described above.

Results and Discussion

Effect of Cu^{2+} mass transfer and concentration on Cu deposition rates.— Figure 1 depicts the effects of $CuSO_4$ concentration and deposition time on Cu film thicknesses determined by AFM. Film thicknesses increase linearly with increasing deposition time for all $CuSO_4$ concentrations up to film thicknesses of ~150 nm. Deposition rates then decrease from these constant values for thicker films, as discussed later. Initial Cu deposition rates, represented by the slopes of the solid lines in Fig. 1, are first-order in $CuSO_4$ concentration (Table I), as was also reported previously.[3,4] The apparent rate constant found here ($\sim 2.7 \times 10^{-3}$ cm s^{-1}) is nearly an order of magnitude greater than the apparent rate constant of 6×10^{-4} cm s^{-1} found previously for deposition onto Si wafers attached to the side of a rotating impeller,[15] demonstrating the influence of mass transfer on Cu deposition rates.

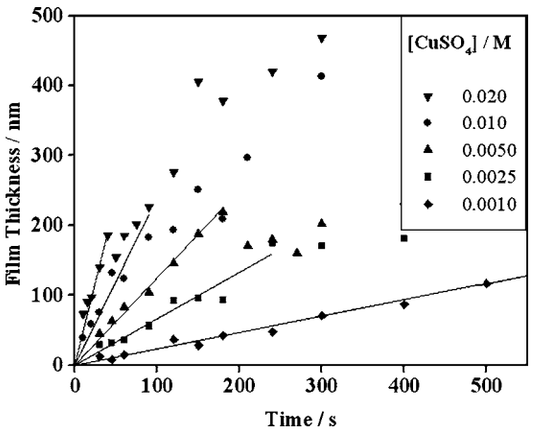

Figure 1. Film thickness evolution during Cu deposition onto Si by galvanic displacement. [HF] = 3.0 M; ω = 50 s^{-1}. The solid lines are best fit lines through the origin for the initial period of constant growth rate, up to 150–200 nm.

RDEs allow mass-transfer effects to be assessed quantitatively, because mass-transfer coefficients can be controlled by varying the electrode rotation speed[28]

$$k_m = 0.62\nu^{-1/6}D_{Cu}^{2/3}\omega^{1/2} \quad [6]$$

where ν is the solution kinematic viscosity, D_{Cu} is the Cu^{2+} diffusion coefficient, and ω is the angular rotation rate. The apparent rate constants shown in Table I are approximately 30% lower than the mass-transfer coefficients calculated for 50 s^{-1} rotation rates using Eq. 6 and assuming $D_{Cu} = 7.2 \times 10^{-6}$ cm^2 s^{-1}.[29,30] This suggests that Cu deposition is under mixed control, with both mass transfer and surface reaction kinetics affecting deposition rates. This is supported by the results in Fig. 2, which show that deposition rates increase with increasing rotation rate but are not proportional to $\omega^{1/2}$, as would be expected if Cu^{2+} diffusion were the only rate-limiting step. Deposition rates approach mass-transfer-limited rates (dashed lines in Fig. 2) at low rotation speeds, when the mass-transfer resistance becomes more significant. This is consistent with previous results, which proposed that deposition rates were limited by mass transfer in stagnant solutions.[4,14,31]

Cu:Si atomic ratio and Si dissolution mechanism.— The reaction mechanism for Si oxidation and dissolution was probed by analyzing the relative rates of Cu deposition and Si dissolution. Dissolution of Si as Si^{2+} (Eq. 2 and 3) deposits one Cu atom for each atom of Si dissolved, while dissolution of Si as Si^{4+} (Eq. 4 and 5) results in a Cu:Si ratio of 2. The rates of Cu deposition and Si

Table I. Effect of $CuSO_4$ concentration on initial deposition rates (film thickness <150 nm) demonstrating first-order dependence.[a]

$[CuSO_4]$/M	Initial deposition rate (nm s^{-1})	Initial deposition rate (10^{-9} mol cm^{-2} s^{-1})	Apparent rate constant[b] (cm s^{-1})
0.0010	0.23	2.6	0.0026
0.0025	0.66	7.4	0.0030
0.0050	1.2	14.0	0.0028
0.010	2.4	27.0	0.0027
0.020	4.8	53.0	0.0027

[a] [HF] = 3.0 M; ω = 50 s^{-1}. Deposition rates in mol cm^{-2} s^{-1} were calculated by assuming void fractions of 0.15 for all Cu films.
[b] k_{app} = rate/$[CuSO_4]$.

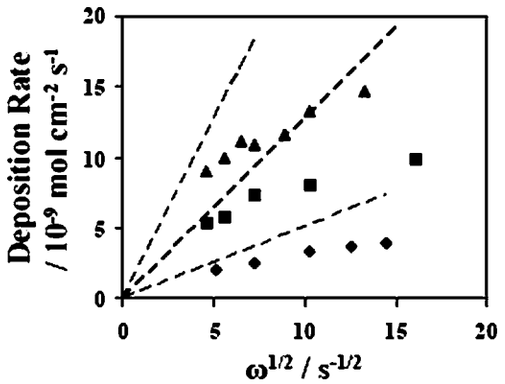

Figure 2. Effect of electrode rotation speed on initial Cu deposition rate at $CuSO_4$ concentrations of (♦) 0.0010, (■) 0.0025, and (▲) 0.0050 M. [HF] = 3.0 M. The dashed lines indicate diffusion-limited rates for each concentration, with the mass-transfer coefficients calculated using Eq. 6, assuming the Cu^{2+} diffusion coefficient is 7.2×10^{-6} cm^2 s^{-1}. Deposition rates were determined from Cu film thicknesses measured by AFM and converted moles by assuming void fractions of 0.15.

dissolution determined from UV-visible spectra were approximately equal for a solution initially containing 3.0 M HF and 0.0025 M $CuSO_4$ (Fig. 3a). The Cu:Si atomic ratio was 1.1 ± 0.2, independent of deposition time (Fig. 3b). This ratio is consistent with Cu:Si ratios determined from weight measurements and from height measurements on Si wafers patterned with SiC, which produced Cu:Si atomic ratios of 1.1 ± 0.4 and 1.2 ± 0.2, respectively. Similar Cu:Si ratios were found when $CuSO_4$ concentrations were varied between

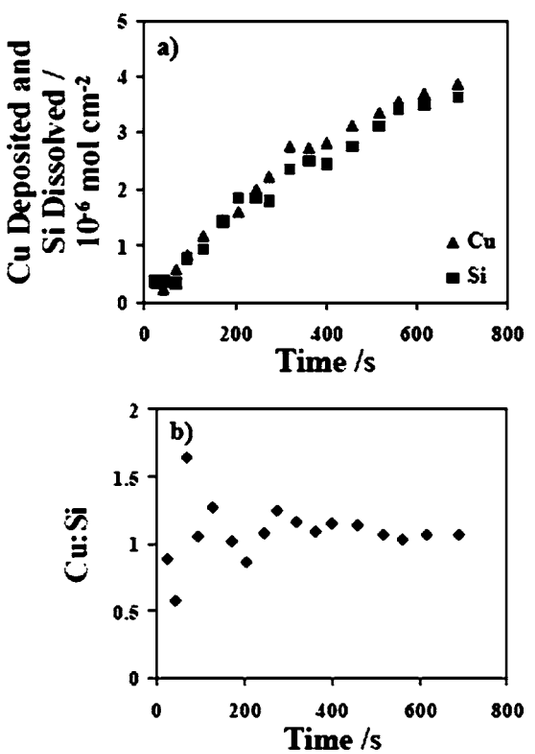

Figure 3. (a) Moles of Cu deposited (▲) and Si dissolved (■) as a function of time, as determined by concentrations measured by UV-visible spectroscopy. [HF] = 3.0 M; [$CuSO_4$] = 0.0025 M; ω = 50 s^{-1}. (b) Cumulative ratio of Cu deposited to Si dissolved. The average value is 1.1 ± 0.2, indicating that Si is dissolved as Si^{2+}.

0.001 and 0.02 M. Cu:Si ratios less than unity may indicate the presence of side reactions such as H^+ reduction, which would oxidize Si without depositing Cu, as has been observed for galvanic displacement on other substrates.[32] These results demonstrate that Si dissolves as Si^{2+} via Eq. 2 and 3, and not as Si^{4+} via Eq. 4 and 5. This conclusion is consistent with previous direct me asurements of Cu:Si atomic ratios[14,15] but differs from the Cu:Si ratio of 2 that is commonly assumed.

Void fractions of Cu films were estimated by comparing deposition rates determined from AFM film thickness measurements with those determined by UV-visible spectroscopy. The film thickness is related to the moles deposited by the following expression

$$\frac{n_{Cu}}{A} = \frac{h_{Cu}\rho_{Cu}(1-\varepsilon)}{M_{Cu}} \quad [7]$$

In Eq. 7, n_{Cu}/A is the density of Cu on the surface (in mol cm^{-2}) determined from UV-visible spectra, h_{Cu} is the Cu film thickness (in cm) determined by AFM, ρ_{Cu} is the density of bulk Cu (8.92 g cm^{-3}), and M_{Cu} is the molar mass of Cu (63.546 g mol^{-1}). Void fractions of ~0.15 were found for all $CuSO_4$ concentrations, and this value was used to calculate deposition rates from AFM film thickness measurements (Table I, Fig. 2). Formation of porous Cu is necessary to grow the thick films that are observed here, because HF must be able to access and dissolve Si for deposition to continue.

Dissolution of Si as Si^{2+} is consistent with previous studies of anodic oxidation and dissolution of Si at the rates measured during galvanic displacement. Si is dissolved as Si^{2+} when oxidation rates are low, because Si^{2+} surface species are dissolved by HF (Eq. 2) more rapidly than they are oxidized to Si^{4+} (Eq. 4).[7,8] In 3.3 M HF at ω = 50 s^{-1}, Chazalviel et al. found that Si^{2+} dissolution was the primary dissolution pathway for current densities lower than ~150 mA cm^{-2}, while Si^{4+} dissolution occurred at higher current densities.[33,34] This maximum rate of Si^{2+} dissolution corresponds to a Cu deposition rate of 7×10^{-7} mol cm^{-2} s^{-1}, which is more than ten times greater than the highest deposition rates measured in this study. Thus, the low Si oxidation rates in our system favor Si^{2+} dissolution followed by further oxidation in solution, as given by Eq. 2 and 3.

Si^{2+} dissolution is also known to occur at lower potentials, while Si^{4+} dissolution occurs at more positive potentials because rate of oxidation (Eq. 4) increases at higher potentials.[7] OCP values during deposition are typically between 0 and −0.2 V (vs NHE), which are much lower than those reported to form Si^{4+} directly during Si oxidation and dissolution on p-type Si wafers. The transition from Si^{2+} to Si^{4+} dissolution occurred at > + 0.4 V in 1 M HF solutions (the most concentrated solution shown) during oxidation of either rotating[33] or stagnant[35,36] Si samples. Thus, the low OCP values measured during galvanic displacement are also consistent with the proposal that Si dissolves as Si^{2+} during galvanic displacement.

A reaction-transport model for Cu galvanic deposition onto Si films.— The data discussed above indicate Cu deposition is under mixed diffusion and surface kinetic control. The apparent order of the overall process involving mass transfer and surface reaction is unity (Table I), which suggests Cu^{2+} reduction kinetics are first-order. Previous kinetic studies have also determined this reaction to be first-order in Cu^{2+} concentration, with rates increasing exponentially with decreasing potential[2,37,38]

$$r_{Cu} = k^{o}_{Cu}(Cu^{2+})_{surface}\exp\left[-\frac{\alpha F}{RT}(E - E^{o}_{Cu})\right] \quad [8]$$

In the above expression, k^{o}_{Cu} is the rate constant under standard conditions ($E = E^{o}_{Cu} = 0.34$ V, $T = 298$ K, species at unit activity) and α is the transfer coefficient.[37] F is Faraday's constant (96,485 C mol^{-1}), R is the gas constant (8.314 J mol^{-1} K^{-1}), T is the temperature in Kelvin, and $(Cu^{2+})_{surface}$ is the Cu^{2+} concentration at the solid Cu surface. At steady state, the Cu^{2+} reduction rate (Eq.

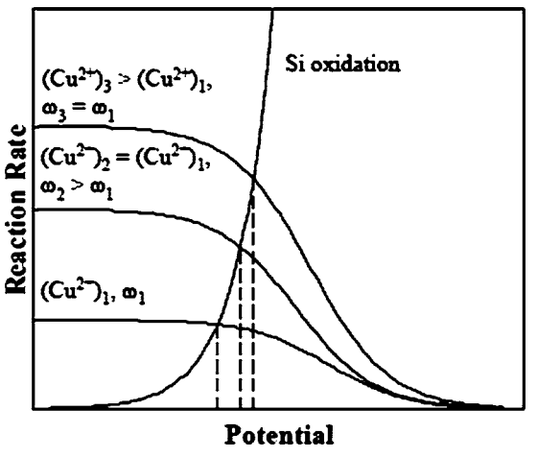

Figure 4. Schematic depiction of the dependence of Cu deposition rates and Si oxidation rates on Cu^{2+} concentration, electrode rotation speed, and potential. The curves for Cu^{2+} reduction were calculated using Eq. 10 and the Si oxidation curve from Eq. 11. The dashed vertical lines mark the intersections of the Cu and Si curves and denote the mixed potential expected in each case.

8) must equal the rate of Cu^{2+} diffusion from the bulk solution to the surface

$$r_{Cu} = 0.62\nu^{-1/6}D_{Cu}^{2/3}\omega^{1/2}[(Cu^{2+})_{bulk} - (Cu^{2+})_{surface}] \quad [9]$$

Equations 8 and 9 can be set equal to each other to solve for the Cu deposition rate by eliminating $(Cu^{2+})_{surface}$

$$r_{Cu} = \frac{0.62\nu^{-1/6}D_{Cu}^{2/3}\omega^{1/2}k_{Cu}^{o}\exp\left[-\frac{\alpha F}{RT}(E - E_{Cu}^{o})\right](Cu^{2+})_{bulk}}{0.62\nu^{-1/6}D_{Cu}^{2/3}\omega^{1/2} + k_{Cu}^{o}\exp\left[-\frac{\alpha F}{RT}(E - E_{Cu}^{o})\right]} \quad [10]$$

Si oxidation (to Si^{2+}) provides the electrons required for Cu^{2+} reduction, and the rates of Si oxidation and dissolution in excess HF were shown previously to increase exponentially with potential[39]

$$r_{Si} = k_{Si}\exp\left[\frac{F}{RT}(E - E_{Si}^{o})\right] \quad [11]$$

Deposition occurs at a mixed potential (E) at which Cu reduction rates (Eq. 10) and Si oxidation rates (Eq. 11) are equal. Rates of Si oxidation and Cu reduction based on Eq. 10 and 11 are shown schematically in Fig. 4. Si oxidation rates increase exponentially with increasing potential and are not limited by diffusion at the rates considered here because of the large excess of HF to Cu^{2+} (>100:1).[33,39] Cu reduction rates increase as the potential decreases before reaching diffusion-limited plateaus. Increasing the driving force for reduction by increasing either the Cu^{2+} concentration or the rotation speed causes the intersection of Cu and Si rates to occur at more positive potentials, as shown in Fig. 4. This increase in mixed potentials occurs for any conditions that increase reduction rates relative to oxidation rates. Conversely, OCP values decrease if the driving force for oxidation increases relative to that for reduction.

Previous work has shown that changes in OCP values with changing solution composition and rotation speed can be used to deduce the rate-limiting steps in each half-reaction.[17] For instance, for Cu reduction rates completely limited by surface kinetics, Eq. 8 describes the Cu^{2+} reduction rate, with the bulk Cu^{2+} concentration replacing the concentration at the electrode surface. The reduction rate given by this expression can then be set equal to the Si oxidation rate in Eq. 11 to give the following potential

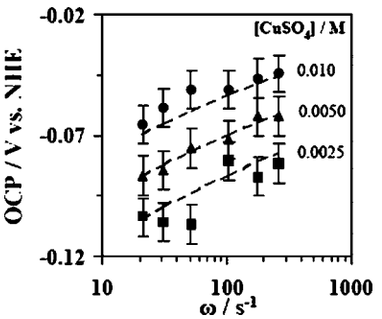

Figure 5. Dependence of OCP at initial stages of deposition on angular velocity and $CuSO_4$ concentration. The dashed lines were calculated by setting the rate of Cu^{2+} reduction in Eq. 10 equal to the rate of Si oxidation in Eq. 11. [HF] = 3.0 M; [$CuSO_4$] = (■) 0.0025, (▲) 0.0050, and (●) 0.010 M.

$$E = \frac{1}{1+\alpha}(\alpha E_{Cu}^{o} + E_{Si}^{o}) + \frac{2.3RT}{(1+\alpha)F}\left[\log\left(\frac{k_{Cu}^{o}}{k_{Si}}\right) + \log(Cu^{2+})\right] \quad [12]$$

This equation predicts that OCP values increase as the logarithm of Cu^{2+} concentration increases, with a slope of approximately 0.04 V per tenfold increase in Cu^{2+} concentration. This mixed potential would also increase if either k_{Cu}^{o} increases or k_{Si} decreases, consistent with the qualitative arguments based on Fig. 4. If Cu^{2+} reduction is instead completely diffusion-limited, the mixed potential is given by[17]:

$$E = E_{Si}^{o} + \frac{2.3RT}{F}\left[\log\left(\frac{0.62\nu^{-1/6}D_{Cu}^{2/3}}{k_{Si}}\right) + \frac{1}{2}\log(\omega) + \log(Cu^{2+})\right] \quad [13]$$

Once again, the potential increases with the logarithm of Cu^{2+} concentration, but in this case the slope is 0.059 V per tenfold change in Cu^{2+} concentration. The dependence on rotation speed gives a slope that is 50% of this value (0.030 V per tenfold change in ω). Conditions leading to mixed control by both diffusion and surface kinetics would result in intermediate values of these slopes.

OCP values measured during Cu deposition increased when either ω or Cu^{2+} concentration increased (Fig. 5), consistent with higher driving forces for the reduction half-reaction. OCP values increased nearly linearly with the logarithm of the rotation rate, with a slope of ~0.022 V per 10-fold change in ω. This slope is somewhat lower than expected from diffusion-limited reduction processes (0.030 V) and is consistent with mixed kinetic and diffusion control. OCP values also increased with the logarithm of Cu^{2+} concentration, with a slope of ~0.054 V per tenfold change in Cu^{2+} concentration. This slope is also between the extreme values for kinetic and diffusion control, as expected based on deposition rate results indicating mixed control.

Mixed-potential theory was used to predict OCP values and deposition rates by solving for the potential E at which the rates of Cu^{2+} reduction (Eq. 10) and Si oxidation (Eq. 11) were equal. Previously reported values were used for D_{Cu}(7.2×10^{-6} cm^2 s^{-1}),[29] k_{Cu}^{o}(3.8×10^{-5} cm s^{-1}),[38] and α (0.46),[38] which left k_{Si} as the only adjustable parameter. The best fit to experimental data was achieved for a k_{Si} value of $(1.0 \pm 0.3) \times 10^{-10}$ cm s^{-1}, which is in reasonable agreement with previous results.[39] OCP values calculated using these parameters effectively capture the effects of both ω and Cu^{2+} concentration on measured OCP values, as shown in Fig. 5. Calculated deposition rates and OCP values are compared with experimental values in Fig. 6a and b, respectively. Both sets of data fall very close to the line $y = x$, indicating good agreement between

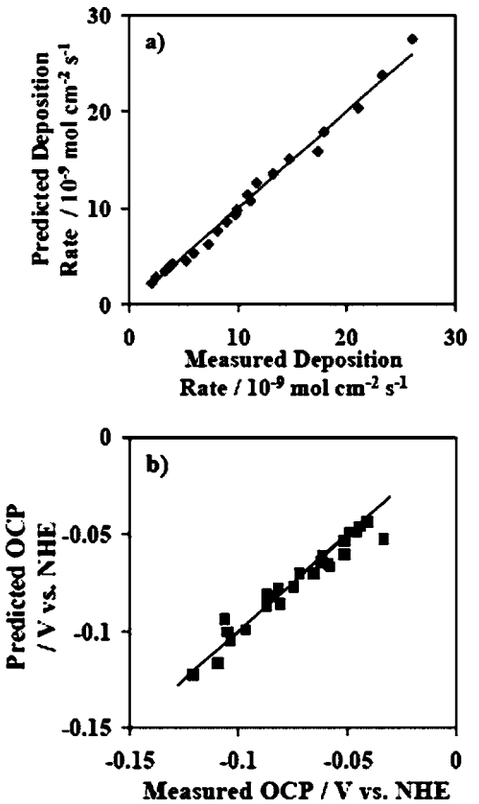

Figure 6. Parity plots comparing initial deposition rates and OCP values predicted using mixed-potential theory with those measured experimentally. Predicted rates and OCP values were calculated by equating rate of Cu^{2+} reduction (Eq. 10) and rate of Si oxidation (Eq. 11). Solid lines in both plots represent the lines $y = x$, indicating complete agreement between experiments and predictions. [HF] = 3.0 M; [$CuSO_4$] = 0.0010–0.020 M; ω = 20–250 s^{-1}. (a) Comparison of measured and predicted deposition rates. (b) Comparison of measured and predicted OCP values.

measured and predicted values over a broad range of $CuSO_4$ concentrations (0.001–0.02 M) and angular velocities (20–250 s^{-1}).

Effects of film thickness on deposition rates.— As discussed above, deposition rates decreased when film thicknesses exceeded ~150 nm for all $CuSO_4$ concentrations (Fig. 1), and deposition rates were no longer accurately predicted by Eq. 10 and 11. OCP values measured during deposition remained nearly constant with deposition time for thin Cu films but then increased as films became thicker than 150 nm (Fig. 7). Higher OCP values reflect an increase in the driving force for reduction relative to that for oxidation. Since these higher OCP values accompany lower deposition rates, we conclude that the driving force for Si oxidation decreased for thicker films.

The presumed products of Si oxidation (SiF_6^{2-}, H_2) were added to deposition solutions to probe whether product inhibition or thermodynamic limitations caused deposition rates to decrease for thicker films. Diffusion of these products through the Cu film becomes slower as film thicknesses increase, which may inhibit deposition by increasing the concentration of these species at the Si surface. Deposition rates were unchanged when 0.1 M H_2SiF_6 was added to solutions containing 3.0 M HF and 0.010 M $CuSO_4$ (Fig. 8). This H_2SiF_6 concentration is more than 10 times larger than the highest SiF_6^{2-} concentration produced during galvanic displacement. Thus, deposition rates are not inhibited by SiF_6^{2-}, and Si oxidation is essentially irreversible.

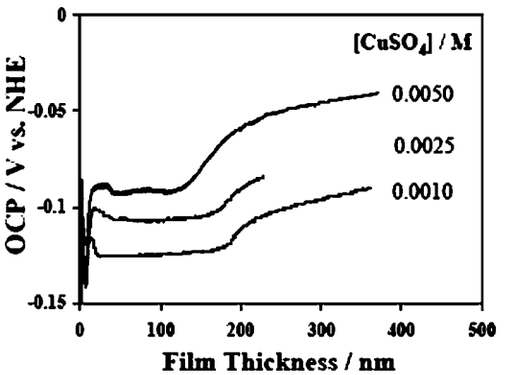

Figure 7. OCP evolution as a function of film thickness for Cu deposition in 0.0010, 0.0050, and 0.020 M $CuSO_4$. In each case, the OCP increases when the film thickness exceeds 150 nm; deposition rates have been found to decrease at this point. [HF] = 3.0 M; angular velocity = 50 s^{-1}.

H_2 formed via reduction of protons coupled with Si oxidation (Eq. 2 and 3) may also inhibit deposition rates, either by decreasing the driving force for oxidation or by forming bubbles that can obstruct access to the surface, as was proposed for Ni deposition on Zn.[5] Bubbling the deposition solution (3.0 M HF, 0.010 M $CuSO_4$) with H_2 (Praxair, 5% H_2/95% N_2) did not influence Cu deposition rates (Fig. 8) or OCP values. This demonstrates that H_2 bubbles trapped within Cu films do not cause deposition rates to decrease for thick films, and processes other than product inhibition must be responsible for these rate decreases.

Deposition rates decreased at similar values of film thickness for all $CuSO_4$ concentrations, rotation speeds, and deposition rates, which suggests that changes in mechanical or structural properties of the film itself may cause deposition rates to decrease. This hypothesis was tested by using optical microscopy to monitor changes in the structure of Cu films during deposition, specifically for film thicknesses exceeding 150 nm. Cu was deposited from stagnant solutions using the experimental setup shown in Fig. 9a, which allowed simultaneous monitoring of OCP values and Cu surface structure. OCP values in a stagnant solution of 3.0 M HF and 0.010 M $CuSO_4$ were nearly constant at −0.14 V vs NHE initially, then abruptly increased after ~500 s (Fig. 9b). This OCP value at short deposition times is lower than those measured on rotating Si samples (Fig. 5), consistent with the lower mass-transfer rates in stagnant solutions. The Cu film thickness is ~150 nm when the OCP increases abruptly (Fig. 9b); this is similar to the thickness at which OCP values increase and deposition rates decrease for rotating Si samples (Fig. 7). Optical micrographs of the Cu surface show

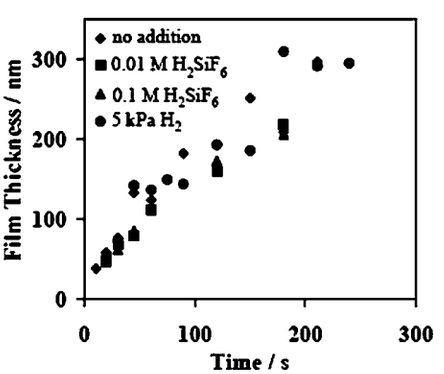

Figure 8. Effect of product inhibition on Cu deposition rates. No product inhibition is observed following addition of (■) 0.01 M H_2SiF_6, (▲) 0.1 M H_2SiF_6, and (●) H_2. [HF] = 3.0 M; [$CuSO_4$] = 0.010 M; ω = 50 s^{-1}.

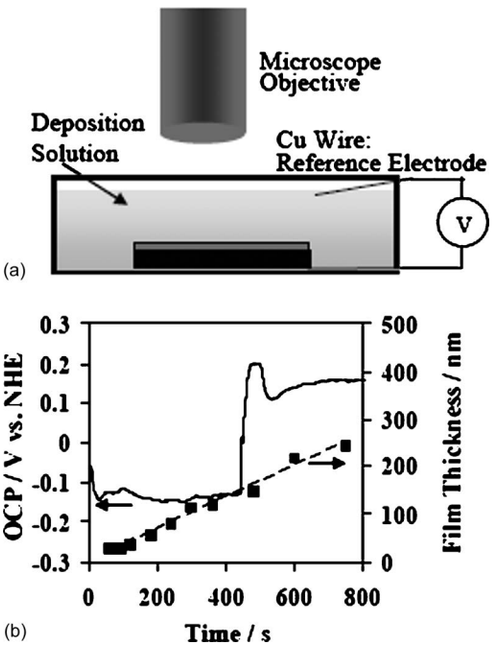

Figure 9. (a) Diagram of experimental setup for simultaneous monitoring of Cu surface and OCP. The deposition solution is stagnant, and the volume of the cuvette is 4 cm^3. (b) Time evolution of OCP and film thickness in stagnant solution; OCP was measured while the Cu surface was monitored by optical microscopy. OCP values increased abruptly at a deposition time of ~500 s, when the film thickness was ~150 nm. The labels on the plot reflect the times at which the images in Fig. 10a-d were captured. [HF] = 3.0 M; [$CuSO_4$] = 0.010 M.

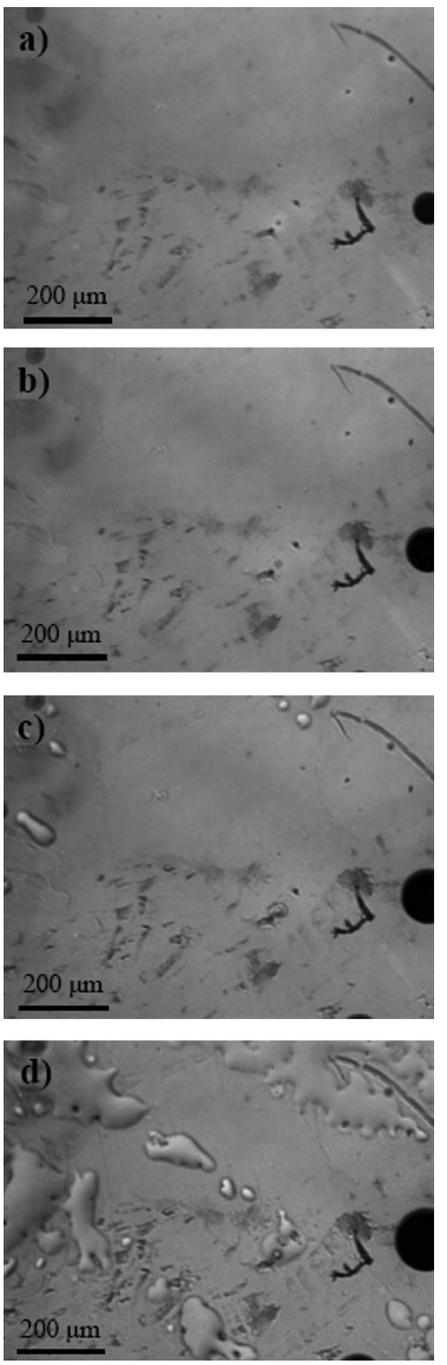

Figure 10. Optical micrographs of Cu surface evolution during deposition in stagnant solution, corresponding to the time evolution of OCP shown in Fig. 9b. These micrographs were taken at (a) 200, (b) 400, (c) 500, and (d) 650 s of deposition. Bulges are seen on the Cu surface in Fig. 10c and d, coinciding with higher OCP values, as shown in Fig. 9b. [HF] = 3.0 M; [$CuSO_4$] = 0.010 M. The black circle on the right is a growing gas bubble on the surface, presumably H_2.

that bulges appeared on the Cu film at the same time as the OCP values increased (Fig. 10), suggesting this structural transformation contributes to the observed OCP shift. Optical micrographs of Cu films following deposition on Si RDEs also revealed bulges on the Cu surface for films thicker than 150 nm. This indicates that the buckling observed in Fig. 10 is not an artifact of the different deposition conditions (Fig. 9a), and the conclusions drawn from film growth in stagnant solutions can be applied to deposition on RDEs.

The buckling observed for thick Cu films (Fig. 10c and d) is likely a response to internal stress within the film. This buckling is similar to delamination that occurred previously for 200 nm Cu films subjected to compressive stress.[40] Compressive stress has been observed previously in Cu films deposited onto Si by electroless deposition.[41] The stresses in these films were relatively low and films did not buckle, perhaps because ethylenediaminetetraacetic acid (EDTA) present in solution chelates Cu^{2+} ions and improves film properties.[42] EDTA is not compatible with the acidic solutions used in this work, but improved film properties have been reported for Cu galvanic displacement in neutral NH_4F solutions, where NH_3 can stabilize Cu^{2+} in solution.[43,44] The effect of these interactions on Cu film properties is a topic for future work.

The detachment of Cu films from the Si substrates decreases deposition rates by decreasing the effective contact area for electron transfer between Cu and Si. Specifically, Cu deposition and Si dissolution rates are expected to decrease in regions where Cu has detached from the Si substrate. This hypothesis was tested by probing the spatial coherence of the Cu deposited and the Si removed using atomic force and optical microscopy of the Cu surface and the underlying Si. An optical micrograph of a region from which Cu was partially removed by abrasion with Teflon tweezers is shown in Fig. 11. The Cu film (on the right side of the image) is rougher near the top of the image than near the bottom. The smoother area near the bottom of the image corresponds to a position where Cu buckled and detached from the Si surface during deposition. The Si surface is also rougher near the top of the image, suggesting more dissolution in this region than at the bottom, where Cu detached. AFM scans confirm that Si dissolution is faster in the rough region, where the average height is ~20 nm lower than the height of the smoother region. The boundary separating rough and smooth Si in Fig. 11 coincides exactly with the boundary between rough and smooth Cu,

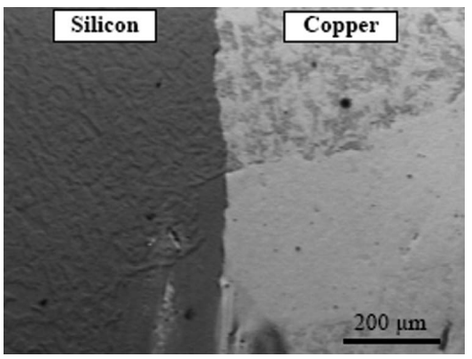

Figure 11. Optical micrograph of a partially removed Cu film on Si. The Cu film on the left side of the image was removed using Teflon tweezers to expose the underlying Si surface. The smooth, lighter area of Cu toward the bottom of the image corresponds to the location where the Cu film detached from the Si surface during deposition (i.e., the bulges seen in Fig. 10c and d). $[HF] = 3.0$ M; $[CuSO_4] = 0.010$ M; film thickness = 300 nm.

indicating the effect of Cu detachment on Si dissolution rates. Cu detachment occurs in the smoother region, and Si dissolution rates decreased upon detachment of the Cu film, demonstrating the importance of local contact between Cu and Si for galvanic displacement.

Buckling in Cu films also decreases the adhesion of thick films, which sometimes delaminate from the Si substrate during drying in N_2, without any mechanical abrasion. Previous studies have also detected poor adhesion and high internal stresses for thick films during Cu deposition on Si.[45] Thus, controlling film stress is critical to improving the properties of Cu films deposited onto Si using galvanic displacement.

Conclusions

Cu was deposited onto Si RDEs to determine the effects of mass transfer and reaction kinetics on galvanic displacement rates. Cu deposition rates are found to be first-order in $CuSO_4$ concentration, and deposition rates are under mixed kinetic and diffusion control. Over the examined range of $CuSO_4$ concentration and rotation speed, the Cu:Si stoichiometry was determined to be 1:1 by three independent methods, namely, UV-visible spectroscopy of concentrations in solution, mass change during deposition, and height changes using Si patterned with SiC. These results indicate Si is dissolved as Si^{2+} under the reaction conditions, not Si^{4+} as is commonly assumed. Mixed-potential theory was used to accurately predict both the rate of Cu deposition and the OCP during galvanic displacement, using parameters found in the literature. This demonstrates the advantage of measuring OCP to monitor changes in rate-limiting processes in real-time. The methods used here are general and can be extended to predict the deposition rate of other metals on Si.

Deposition rates decreased when film thicknesses exceeded 150 nm for all $CuSO_4$ concentrations and mass-transfer rates were studied. This rate decrease was accompanied by an increase in the OCP, suggesting it is caused by a decrease in the oxidation rate. Concentration gradients of HF, SiF_6^{2-}, and H_2 within the Cu film were not responsible for the rate decrease. Optical and atomic force microscopy revealed Cu films buckled and partially detached from Si at the same time that OCP values increased abruptly. Si dissolution rates decreased beneath the detached Si, as the lower Cu–Si contact area slowed electron transfer from Si to Cu. Thus, film stress was found to strongly affect the film structure, Cu–Si adhesion, and the deposition rate.

Acknowledgments

The authors thank Professor Elton Cairns for the use of the rotating disk electrode. Financial support from the Committee on Research of the University of California at Berkeley and the National Science Foundation is gratefully acknowledged. C.d'R. also thanks the National Science Foundation and Chevron Foundation for graduate fellowships.

The University of California, Berkeley, assisted in meeting the publication costs of this article.

References

1. J. O. Bockris and M. Enyo, *Trans. Faraday Soc.*, **58**, 1187 (1962).
2. E. Mattsson and J. O. Bockris, *Trans. Faraday Soc.*, **55**, 1586 (1959).
3. M. K. Lee, H. D. Wang, and J. J. Wang, *Solid-State Electron.*, **41**, 695 (1997).
4. L. Torcheux, A. Mayeux, and M. Chemla, *J. Electrochem. Soc.*, **142**, 2037 (1995).
5. L. Makhloufi, B. Saidani, C. Cachet, and R. Wiart, *Electrochim. Acta*, **43**, 3159 (1998).
6. G. P. Power, W. P. Staunton, and I. M. Ritchie, *Electrochim. Acta*, **27**, 165 (1982).
7. R. Memming and G. Schwandt, *Surf. Sci.*, **4**, 109 (1966).
8. M. J. Eddowes, *J. Electroanal. Chem. Interfacial Electrochem.*, **280**, 297 (1990).
9. M. M. Rieger and P. A. Kohl, *J. Electrochem. Soc.*, **142**, 1490 (1995).
10. D. R. Turner, *J. Electrochem. Soc.*, **105**, 402 (1958).
11. O. M. R. Chyan, J. J. Chen, H. Y. Chien, J. Sees, and L. Hall, *J. Electrochem. Soc.*, **143**, 92 (1996).
12. J. S. Jeon, S. Raghavan, H. G. Parks, J. K. Lowell, and I. Ali, *J. Electrochem. Soc.*, **143**, 2870 (1996).
13. G. Li, E. A. Kneer, B. Vermeire, H. G. Parks, S. Raghavan, and J. S. Jeon, *J. Electrochem. Soc.*, **145**, 241 (1998).
14. S. G. dos Santos, L. F. O. Martins, P. C. T. D'Ajello, A. A. Pasa, and C. M. Hasenack, *Microelectron. Eng.*, **33**, 59 (1997).
15. S. G. dos Santos, A. A. Pasa, and C. M. Hasenack, *Microelectron. Eng.*, **33**, 149 (1997).
16. P. Gorostiza, M. A. Kulandainathan, R. Diaz, F. Sanz, P. Allongue, and J. R. Morante, *J. Electrochem. Soc.*, **147**, 1026 (2000).
17. G. P. Power and I. M. Ritchie, *Electrochim. Acta*, **26**, 1073 (1981).
18. C. Wagner and W. E. Traud, *Z. Elektrochem. Angew. Phys. Chem.*, **44**, 391 (1938).
19. W. Y. Wei, C. Lee, and H. J. Chen, *Langmuir*, **10**, 1980 (1994).
20. V. Bertagna, C. Plougonven, F. Rouelle, and M. Chemla, *J. Electrochem. Soc.*, **143**, 3532 (1996).
21. F. A. Harraz, J. Sasano, T. Sakka, and Y. H. Ogata, *J. Electrochem. Soc.*, **150**, C277 (2003).
22. W. C. Ye, Y. L. Chang, C. L. Ma, B. Y. Jia, G. Y. Cao, and C. M. Wang, *Appl. Surf. Sci.*, **253**, 3419 (2007).
23. T. Ohmi, T. Imaoka, I. Sugiyama, and T. Kezuka, *J. Electrochem. Soc.*, **139**, 3317 (1992).
24. I. Teerlinck, P. W. Mertens, H. F. Schmidt, M. Meuris, and M. M. Heyns, *J. Electrochem. Soc.*, **143**, 3323 (1996).
25. Z. Marczenko, *Separation and Spectrophotometric Determination of Elements*, p. 516, Halsted Press, New York (1986).
26. D. Gao, R. T. Howe, and R. Maboudian, *Appl. Phys. Lett.*, **82**, 1742 (2003).
27. M. B. J. Wijesundara, G. Valente, W. R. Ashurst, R. T. Howe, A. P. Pisano, C. Carraro, and R. Maboudian, *J. Electrochem. Soc.*, **151**, C210 (2004).
28. V. G. Levich, *Physicochemical Hydrodynamics*, Prentice-Hall, Englewood Cliffs, NJ (1962).
29. J. Newman and K. E. Thomas-Alyea, *Electrochemical Systems*, Wiley, Hoboken, NJ (2004).
30. T. I. Quickenden and Q. Z. Xu, *J. Electrochem. Soc.*, **143**, 1248 (1996).
31. E. Hsu, H. G. Parks, R. Craigin, S. Tomooka, J. S. Ramberg, and R. K. Lowry, *J. Electrochem. Soc.*, **139**, 3659 (1992).
32. J. A. P. Mathes, F. Lawson, and D. R. Canterford, *Hydrometallurgy*, **14**, 1 (1985).
33. J. N. Chazalviel, M. Etman, and F. Ozanam, *J. Electroanal. Chem. Interfacial Electrochem.*, **297**, 533 (1991).
34. M. Etman, M. Neumannspallart, J. N. Chazalviel, and F. Ozanam, *J. Electroanal. Chem. Interfacial Electrochem.*, **301**, 259 (1991).
35. W. R. Thurber, R. L. Mattis, Y. M. Liu, and J. J. Filliben, *J. Electrochem. Soc.*, **127**, 2291 (1980).
36. X. G. Zhang, S. D. Collins, and R. L. Smith, *J. Electrochem. Soc.*, **136**, 1561 (1989).
37. A. J. Bard and L. R. Faulkner, *Electrochemical Methods: Fundamentals and Applications*, Wiley, New York (2001).
38. J. T. Hinatsu and F. R. Foulkes, *Can. J. Chem. Eng.*, **69**, 571 (1991).
39. P. C. Searson and X. G. Zhang, *J. Electrochem. Soc.*, **137**, 2539 (1990).
40. J. W. Hutchinson, M. D. Thouless, and E. G. Liniger, *Acta Metall.*, **40**, 295 (1992).
41. N. Fukumuro, M. Yamazaki, K. Ito, H. Ishihara, S. Kakunai, S. Yae, and H. Matsuda, *Electrochem. Solid-State Lett.*, **10**, E14 (2007).
42. R. Pauliukaite, G. Stalnionis, Z. Jusys, and A. Vaskelis, *J. Appl. Electrochem.*, **36**, 1261 (2006).
43. L. Magagnin, R. Maboudian, and C. Carraro, *Electrochem. Solid-State Lett.*, **4**, C5 (2001).
44. L. Magagnin, R. Maboudian, and C. Carraro, *Thin Solid Films*, **434**, 100 (2003).
45. S. Bhansali, D. K. Sood, and R. B. Zmood, *Thin Solid Films*, **253**, 391 (1994).